DFSs, either by looking at three- and four-photon events or, more easily, by using more degrees of freedom of the photon pairs (*23, 24*). For example, one might employ the entangled spatial modes to represent additional qubits while relying on frequency techniques to produce decoherence. Finally, we can extend our investigations to include dissipation by introducing controllable polarization-dependent losses.

References and Notes

1. P. W. Shor, in *Proceedings of the 35th Annual Symposium on Foundations of Computer Science*, S. Goldwasser, Ed. (IEEE Computer Society, Los Alamitos, CA, 1994), p. 116.
2. R. Feynman, *Int. J. Theor. Phys.* **21**, 467 (1982).
3. S. Somaroo, C. H. Tseng, T. F. Havel, R. Laflamme, D. G. Cory, *Phys. Rev. Lett.* **82**, 5381 (1999).
4. L. K. Grover, *Phys. Rev. Lett.* **79**, 325 (1997).
5. N. J. Cerf, L. K. Grover, C. P. Williams, *Phys. Rev. A* **61**, 32303 (2000).
6. D. Gottesman, *Phys. Rev. A* **54**, 1862 (1996).
7. C. H. Bennett, P. W. Shor, *IEEE Trans. Inf. Theory* **44**, 2724 (1998).
8. L. Viola, E. Knill, S. Lloyd, *Phys. Rev. Lett.* **82**, 2417 (1999).
9. G. M. Palma, K.-A. Suominen, A. K. Ekert, *Proc. R. Soc. London Ser. A* **452**, 567 (1996).
10. L.-M. Duan, G.-C. Guo, *Phys. Rev. Lett.* **79**, 1953 (1997).
11. P. Zanardi, M. Rasetti, *Phys. Rev. Lett.* **79**, 3306 (1997).
12. D. A. Lidar, I. L. Chuang, K. B. Whaley, *Phys. Rev. Lett.* **81**, 2594 (1998).
13. P. Zanardi, *Phys. Rev. A* **60**, R729 (1999).
14. D. Bacon, D. A. Lidar, K. B. Whaley, *Phys. Rev. A* **60**, 1944 (1999).
15. J. Kempe, D. Bacon, D. A. Lidar, K. B. Whaley, E-print available at http://xxx.lanl.gov/abs/quant-ph/0004064.
16. A. Beige, D. Braun, B. Tregenna, P. L. Knight, *Phys. Rev. Lett.* **85**, 1762 (2000).
17. R. Jozsa, *J. Mod. Opt.* **41**, 2315 (1994).
18. E. Knill, R. Laflamme, L. Viola, *Phys. Rev. Lett.* **84**, 2525 (2000).
19. P. G. Kwiat, E. Waks, A. G. White, I. Appelbaum, P. H. Eberhard, *Phys. Rev. A.* **60**, R773 (1999).
20. M. Born, E. Wolf, *Principles of Optics* (Cambridge Univ. Press, Cambridge, 1999).
21. A. G. White, D. F. V. James, P. H. Eberhard, P. G. Kwiat, *Phys. Rev. Lett.* **83**, 3103 (1999).
22. A. J. Berglund, thesis, Dartmouth College, Hanover, NH (2000) (E-print available at http://xxx.lanl.gov/abs/quant-ph/0010001).
23. P. G. Kwiat, *J. Mod. Opt.* **44**, 2173 (1997).
24. _____, J. R. Mitchell, P. D. D. Schwindt, A. G. White, *J. Mod. Opt.* **47**, 257 (2000).

25. We thank S. Barraza-Lopez and D. James for assistance and D. Lidar and L. Viola for valuable discussions. This work was supported in part by the National Security Agency and Advanced Research and Development Activity (ARDA) under contract MOD-713700.

13 June 2000; accepted 29 August 2000

Electronic Structure of Solids with Competing Periodic Potentials

J. Voit,[1]* L. Perfetti,[2] F. Zwick,[2] H. Berger,[2] G. Margaritondo,[2] G. Grüner,[3] H. Höchst,[4] M. Grioni[2]*

When electrons are subject to a potential with two incommensurate periods, translational invariance is lost, and no periodic band structure is expected. However, model calculations based on nearly free one-dimensional electrons and experimental results from high-resolution photoemission spectroscopy on a quasi–one-dimensional material do show dispersing band states with signatures of both periodicities. Apparent band structures are generated by the nonuniform distribution of electronic spectral weight over the complex eigenvalue spectrum.

One of the basic tenets of solid state physics is that the periodicity of the crystal lattice determines the electronic structure (*1*). The band structure of a crystalline solid differs from the free-electron dispersion $E(k) = \hbar^2k^2/2m$ (k, wave vector; $\hbar$, Planck's constant divided by 2π; m, electron mass) most fundamentally by the effects of Bragg reflection on the crystal lattice, which opens gaps at the Brillouin zone (BZ) boundaries and folds back dispersion branches into the first BZ (1BZ). The complete band structure can then be represented equivalently in the reduced, extended, or repeated zone schemes. By contrast, genuine aperiodic (glassy or amorphous) systems would not show dispersing bands.

Important questions for the understanding of band structures are, What are the states of electrons in quasiperiodic systems, or in a potential with two competing, incommensurate periodicities? Are they still periodic? What would experimental probes of "band structures," such as angle-resolved photoemission spectroscopy (ARPES), observe? If the two periodicities Q_1 and Q_2 are commensurate (Q_1/Q_2 is a rational number) or can be reduced to a commensurate approximant, one can recover a consistent description of the electronic structure in the reduced 1BZ of the longer periodicity, although even here, the relevance of this reduced zone for experiments is unclear. More delicate is the case where the two potentials are truly incommensurate (Q_1/Q_2 is an irrational number). Typical examples are quasi–one-dimensional Peierls systems where, below a critical temperature T_P, a lattice modulation and an electronic charge-density wave (CDW) with twice the Fermi wave number ($2k_F$, unrelated to the lattice periodicity) form because of electron-phonon coupling (*2*).

With two incommensurate periods, translational invariance is lost, and the electronic states can no longer be classified according to wave numbers k. One expects a hierarchy of energy levels whose distribution will depend, among other factors, on the periods of the potential. Such level schemes have been calculated for a few theoretical problems, the most famous being the Hofstadter butterfly spectrum of two-dimensional electrons in a magnetic field (*3*). Other examples include one-dimensional (1D) quasicrystals (*4*) or soliton states in 1D Peierls models (*5*). However, it is not clear that such complex nondispersive level structures can be observed directly. X-ray diffraction of incommensurate structures still gives sharp peaks, so that the two underlying periodicities are correctly "recognized." The two problems, however, are not equivalent. The x-ray pattern is the Fourier transform of the electronic density distribution, whereas no similar relation exists for the electronic structure.

Using a simple model of 1D electrons in incommensurate potentials, we show that, despite the collapse of the BZ, the spectral weight of photoelectrons is peaked at "bands" close to the free-electron parabola. In an extended zone scheme, these bands are modulated by the strength of the potentials and exhibit gaps at the appropriate wave vectors. We find similar structures in high-resolution ARPES experiments on a typical 1D Peierls material, $(TaSe_4)_2I$. We observe, however, additional subtleties, which we explain with a model specific to $(TaSe_4)_2I$.

First, we consider 1D tight-binding electrons (lattice constant a; $Q_1 = 2\pi/a$) in a superstructure with a commensurate period $4a$ ($Q_2 = \pi/2a$). Such a superstructure could arise from a Peierls transition in a quarter-filled conduction band. The Hamiltonian is

[1]Theoretische Physik 1, Universität Bayreuth, D-95440 Bayreuth, Germany. [2]Institut de Physique Appliquée, Ecole Polytechnique Fédérale, CH-1015 Lausanne, Switzerland. [3]Department of Physics, University of California, Los Angeles, CA 90095–1547, USA. [4]Synchrotron Radiation Center, University of Wisconsin–Madison, Stoughton, WI 53589–3097, USA.

*To whom correspondence should be addressed. E-mail: johannes.voit@uni-bayreuth.de (J.V.) and marco.grioni@epfl.ch (M.G.)

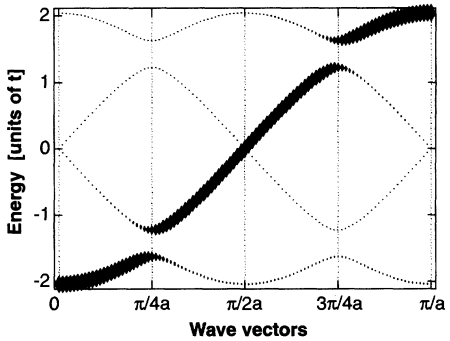

Fig. 1. Spectral weight distribution of 1D tight-binding electrons in superstructure with period 4. The size of the symbols is proportional to the spectral weight when it is above 0.1 and is constant below 0.1. The hopping matrix element is $t = 1$, and the potential amplitude is $V = 0.2t$.

$$H = \sum_{k,s} \left\{ \varepsilon(k) c_{ks}^{\dagger} c_{ks} + \sum_{q} [V(q) c_{k+qs}^{\dagger} c_{ks} + \text{H.c.}] \right\} \quad (1)$$

The kinetic energy is $\varepsilon(k) = -2t \cos(ka)$, the potential is $V(q) = V\delta_{q,Q_2}$, and c_{ks} describes electrons with momentum k and spin s (H.c., Hermitian conjugate). Because $4Q_2$ is a reciprocal lattice vector, the Hamiltonian is a 4-by-4 matrix, which is readily diagonalized. Photoemission measures the single-particle spectral function $\rho(k, \omega)$ depending on wave vector k and frequency ω, which we express as

$$\rho[k + (i-1)Q_2, \omega] = \sum_{j=1}^{4} [x_j(k)]_i^2 \, \delta[\omega - E_j(k)],$$

$$i = 1, \ldots, 4, \quad -\frac{\pi}{4a} \le k \le \frac{\pi}{4a} \quad (2)$$

in terms of the components of the eigenvectors x_j associated with the eigenvalues E_j of the Hamiltonian δ [. . .] is Dirac's delta function. Figure 1 shows this spectral function, i.e., the dispersion and the spectral weight distribution of the electronic states. The latter is proportional to the photoemission (inverse photoemission) intensity when the corresponding states are occupied (unoccupied). Gaps appear at wave vectors $(n + 1/2)Q_2$. The dispersion of the eigenvalues follows the repeated zone scheme, but the spectral weight is concentrated on the extended zone scheme dispersion. The weight transferred away from it depends on the ratio Δ/W, where Δ is (half) the gap and W is the bandwidth. For a superstructure with period 2, the weight factors in Eq. 2 reduce to the coherence factors $u_k^2, v_k^2 = [1 \pm \varepsilon(k)/|E(k)|]/2$, as in the theory of superconductivity.

We now consider the more general case of nearly free 1D electrons in a potential with incommensurate wave vectors Q_1 and Q_2.

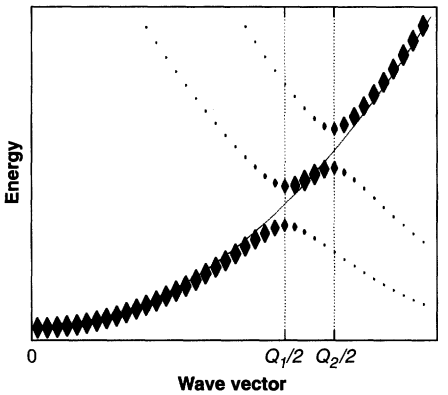

Fig. 2. Spectral weight distribution of 1D electrons in a potential with two incommensurate wave vectors Q_1 and $Q_2 = (5^{1/2} - 1)Q_1$. The size of the symbols indicates the spectral weight, as in Fig. 1. The electron mass is $m = 1$, and the potentials are $V_1 = V_2 = 0.05$.

Again, for a Peierls system, Q_1 may be related to the high-temperature crystal structure, and $Q_2 = 2k_F = \pi\rho/a$ would depend on the band-filling $\rho = N_{el}/N_{site}$, i.e., the number of electrons per site. An exact solution of Eq. 1 with $\varepsilon(k) = \hbar^2k^2/2m$ and $V(q) = V_1\delta_{q,Q_1} + V_2\delta_{q,Q_2}$ is no longer feasible because the matrix now has infinite dimension. We truncate the Hamiltonian at order n, where a state k is coupled to all states $k + rQ_1 + sQ_2$ with $|r| + |s| \le n$. The band structure and spectral weight distribution obtained by diagonalizing the Hamiltonian truncated at first order are shown in Fig. 2. The spectral weight is concentrated on the free-electron parabola, and the potential opens gaps at $Q_1/2$ and $Q_2/2$ and generates new, weak bands that bend backward from the gap edges. Unlike the commensurate case, these shadow bands cannot be described in a repeated zone scheme. With increasing n, an increasing number of bands and gaps with sizes exponentially small in n appear on the electronic dispersion. For the weak superstructures considered in our calculation, even for $n = 2$, these additional gaps are too small, and the intensity redistribution that they induce is too weak to be visible on the scale of Fig. 2. Also, calculations with commensurate approximants suggest that a first-order truncation gives a good representation when the potential amplitudes are weak. The numerous exponentially small "baby gaps" and the fractal structure expected in the incommensurate limit (*6*) then are essentially invisible. These results are of wider validity than Peierls systems. Specifically, they also apply to 1D quasicrystals whose properties are deduced from solving commensurate approximant structures (*4*).

When electronic weight factors are disregarded and the eigenvalues of our Hamiltonian are traced out, one recovers the nondispersive level schemes, i.e., the local densities of states discussed in the literature (*4, 6*). The modulation of these densities brought in by the piling up of the electronic spectral weight close to the "bands" of the extended zone scheme reintroduces dispersion, despite the absence of periodicity. The physical origins are most clearly seen by considering a commensurate approximant. Here, a period n superstructure on the one hand is responsible for the n-fold folding of the band structure into the 1BZ; on the other hand, it also provides a multitude of reciprocal lattice vectors for Bragg scattering into higher BZs. Our calculations show that the most important of those processes at a given energy are those that bring the weight back to the free-electron parabola.

The Peierls system $(TaSe_4)_2I$ is a good candidate for the verification of these predictions. This material has strongly anisotropic properties (*7*), due to a 1D electronic band formed on $TaSe_4$ chains with a lattice constant $c = 12.824$ Å; $c = 4a$, where a is the Ta-Ta distance (and the notation of Fig. 1), because of the periodic arrangement of the Se_4 units around the Ta chain. In a purely ionic picture, 0.5 electron would be transferred from each Ta d^1 atom to the I ions, and the conduction band would be quarter filled, i.e., $k_F = \pi/c = 0.245$ Å^{-1}. However, the charge transfer between Ta and I is incomplete. The Ta-d_{z^2} band is effectively "electron doped," and $k_F > \pi/c$ (*8*). Below $T_P = 263$ K, the system is in a CDW state (*9*). X-ray scattering shows a small deviation of k_F from commensurability by $0.085\pi/c$ (*10*). We performed high-resolution ($\Delta E = 10$ meV and $\Delta k \sim 0.04$ Å^{-1}) ARPES experiments on high-quality single crystals with atomically clean flat surfaces (*11*). We measured a temperature at 300 K just above T_P, but because of strong precursor fluctuations, the CDW gap is almost completely developed at this temperature (*12*).

The intensity map (Fig. 3A) summarizes the ARPES data for a large wave vector range along the chain direction. The color coding reproduces the photoelectron intensity normalized, for each k vector, to the acquisition time. A strong band disperses throughout the 1BZ and peaks near the zone boundaries $\pm\pi/c$. The line shape (not shown in Fig. 3A) has a sharp peak with broad tails, as in $(NbSe_4)_3I$ (*13*). We also observe a weaker replica (or shadow) of this band centered at the Γ' point, shifted by $2\pi/c$, and even a second, faint replica around the Γ'' point, shifted by $4\pi/c$ from Γ. (Γ, Γ', and Γ'' label the centers of the first, second, and third BZs, respectively.) The low intensity at E_F for wave vectors close to k_F is indicative of a deep pseudogap (*14–16*). There is consistency in the gap values with other experiments if half the gap is defined by the extrapolation of the leading edge of the ARPES line shape (*13*). Then, the "bad metal" state of $(TaSe_4)_2I$ at $T > T_P$ is identified by this extrapolation intersecting the baseline at the chemical potential, whereas it intersects at a finite binding energy in the CDW phase. A determination of (pseudo)gap sizes based on peak positions (*17*) apparently is not permissible in 1D materials.

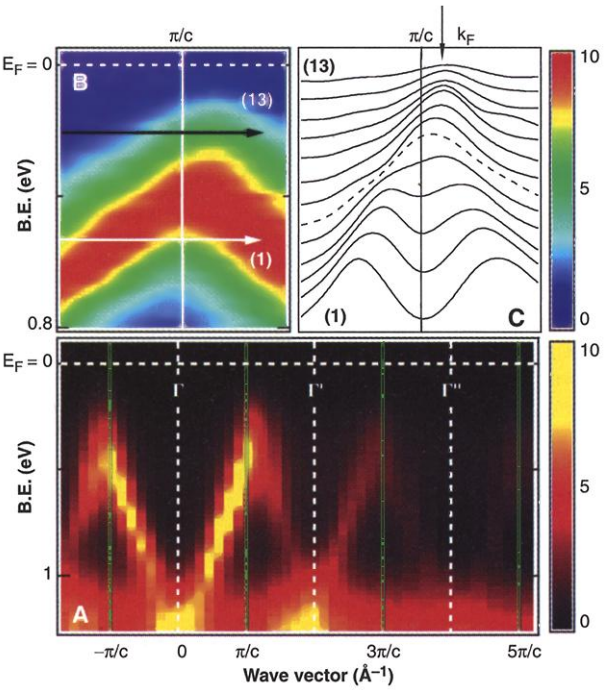

Fig. 3. (**A**) ARPES intensity map [light $h\nu = 21.2$ eV (h is Planck's constant and ν is photon frequency); $T = 300$ K] of $(TaSe_4)_2I$ along the 1D chain direction. B.E., binding energy. (**B**) Detailed view of the region near the zone boundary. For clarity, the raw spectra have been normalized to the same peak intensity and interpolated with respect to energy and wave vector. (**C**) Constant-energy cuts through the intensity map shown in (B), taken at equal energy intervals between the lines marked 1 and 13. The dashed line is a cut at the minimum peak binding energy $E = E^*$.

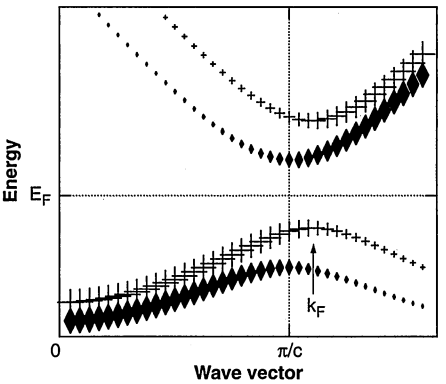

Fig. 4. Dispersion and spectral weight distribution for a slightly doped Peierls ladder. Extrema occur at $Q_1/2 = \pi/c$ and $Q_2/2 = k_F$, analogous with the ARPES results for $(TaSe_4)_2I$ of Fig. 3. The size of the symbols represents the spectral weight, as in Fig. 1.

A dense sampling of the minimal binding energy range near π/c (Fig. 3B) shows that the second periodicity is also present in the band structure, because the turning points at the top and bottom of the ARPES intensity plot do not coincide. More specifically, the turning point at the lower edge is at $k = \pi/c \equiv Q_1/2$, and the turning point at the upper edge is at $k = k_F \equiv Q_2/2$. This is confirmed by constant-energy cuts through the intensity map (Fig. 3C). For large binding energies $E < E^*$, two peaks (i.e., a band and its shadow) disperse symmetrically toward $Q_1/2$ to a minimum peak binding energy E^* (dashed curve), where they merge. For $E > E^*$, a single peak disperses further toward the chemical potential until it reaches $Q_2/2$. We did observe a symmetric behavior at $k = -\pi/c$ (not shown in Fig. 3C), whereas the much weaker intensity forbids a similar fine analysis at the turning points of the shadow bands. The two periodicities observed by ARPES precisely agree with x-ray results (*10*). They become consistent with band structure calculations (*8*) only if the latter are reinterpreted in the extended zone scheme.

The experimental spectrum contains the basic features of Fig. 2. We observe dispersion maxima coming from the two periodicities, at the expected locations in k space. One periodicity (Q_1), however, is clearly predominating, and we observe it over an extended range of k vectors, despite the system being nonperiodic in a strict sense. The Q_2 periodicity is only revealed near the top of the dispersion, and there is no extended counterpart in the higher BZs. Apparently, the puzzle of the two competing periods is resolved by the unequal distribution of spectral weight over the electronic bands. Although band structure calculations usually determine only the eigenvalues of the Hamiltonian, with ARPES, one can observe both the eigenvalues and their weight, obtained from the eigenvectors. There are some subtleties in the ARPES spectrum of $(TaSe_4)_2I$, which cannot directly be addressed by our model of one electronic band subject to two incommensurate potentials. The intensity of the shadow bands in the second and higher BZs is indicative of a strong potential with period Q_1 and a large gap at π/c. From such a strong potential, we then expect strong shadows of the band states between $Q_1/2$ and $Q_2/2$, in the momentum range $(Q_1 - Q_2/2, Q_1/2)$ for which we have no evidence.

A more detailed analysis would consider the specific properties of the material. Analogous to $(NbSe_4)_3I$ (*13*), the ARPES line can be decomposed into two separate features ~0.25 eV apart. The presence of two chains per unit cell (*8*) suggests a two-leg ladder of $TaSe_4$ as the basic building block of the system. The two ARPES features then are naturally associated with the bonding and antibonding ladder states. Such a Peierls ladder may be in a regime where each of the two incommensurate potentials of the superstructure couples to one ladder band separately and where one of the periods remains commensurate with the crystal lattice. The spectral function of this model is calculated by a direct generalization of Eqs. 1 and 2 to ladder systems. The band dispersion and spectral weight distribution for such a situation (Fig. 4) are indeed consistent with the experiment.

Whereas band structure calculations always exhibit the full translational invariance of the crystal potential, this is not necessarily true for experiment. There can be cases where the system is strictly periodic but the spectral weight is not, and what is left of periodicity is the dispersion of weak shadow bands. Conversely, systems that are nonperiodic in a strict sense may exhibit hints of periodicity because of the k-dependent weight in the shadow bands. ARPES shows that this situation is realized in 1D Peierls compounds like $(TaSe_4)_2I$. Fine details of our experiment suggest, however, that the two potentials are coupled to the bonding and antibonding ladder bands separately. We predict that similar dispersing electronic states ought to be observed in 1D quasicrystals.

References and Notes

1. N. W. Ashcroft, N. D. Mermin, *Solid State Physics* (Holt, Rinehart, and Winston, New York, 1976).
2. G. Grüner, *Density Waves in Solids* (Addison-Wesley, Reading, MA, 1994).
3. D. R. Hofstadter, *Phys. Rev. B* **14**, 2239 (1976).
4. F. Piéchon, M. Benakli, A. Jagannathan, *Phys. Rev. Lett.* **74**, 5248 (1995).
5. M. Nakano, K. Machida, *Phys. Rev. B* **33**, 6718 (1986).
6. H. Hiramoto, M. Kohmoto, *Int. J. Mod. Phys. B* **6**, 281 (1992).
7. H. P. Geserich, G. Scheiber, M. Dürrer, F. Levy, P. Monceau, *Physica B* **143**, 198 (1986).
8. P. Gressier, M.-H. Whangbo, A. Meerschaut, J. Rouxel, *Inorg. Chem.* **23**, 1221 (1984).
9. P. Monceau, Ed., *Electronic Properties of Inorganic Quasi–One-Dimensional Compounds* (Reidel, Dordrecht, Netherlands, 1985).
10. H. Fujishita, M. Sato, S. Hoshino, *Solid State Commun.* **49**, 313 (1984).
11. ARPES experiments were performed both in the Electronic Materials Physics Laboratory at Lausanne and at the Synchrotron Radiation Center (SRC) of the University of Wisconsin.
12. L. Degiorgi *et al.*, *Phys. Rev. B* **52**, 5603 (1995).
13. V. Vescoli *et al.*, *Phys. Rev. Lett.* **84**, 1272 (2000).
14. B. Dardel *et al.*, *Phys. Rev. Lett.* **67**, 3144 (1991).
15. Y. Hwu *et al.*, *Phys. Rev. B* **46**, 13624 (1992).
16. R. Claessen *et al.*, *Phys. Rev. B* **56**, 12643 (1997).
17. N. Shannon, R. Joynt, *J. Phys. Condens. Matter* **8**, 10493 (1996).

18. We acknowledge discussions with R. Claessen, L. Forro, D. Malterre, and A. Pasquarello. This work has been supported by the Swiss National Science Foundation and by the Deutsche Forschungsgemeinschaft through a Heisenberg fellowship and grant VO 436/7-1 to J.V. The SRC is funded by the NSF through grant DMR-95-31009.

15 June 2000; accepted 6 September 2000